

# A Spectroscopic Study of the Blue Stragglers in M67

G. Q. Liu,<sup>1,2\*</sup> L. Deng,<sup>1†</sup> M. Chávez,<sup>3‡</sup> E. Bertone,<sup>3§</sup> A. Herrero Davo,<sup>4¶</sup>  
and M. D. Mata-Chávez<sup>5</sup>

<sup>1</sup>NAOC – National Astronomical Observatories, Chinese Academy of Sciences, Beijing 100012, P. R. China

<sup>2</sup>GUCAS – Graduate University of Chinese Academy of Sciences, Beijing 100049, P. R. China

<sup>3</sup>INAOE – Instituto Nacional de Astrofísica, Óptica y Electrónica, Luis Enrique Erro 1, 72840 Tonantzintla, Puebla, Mexico

<sup>4</sup>IAC – Instituto de Astrofísica de Canarias, E38205 La Laguna, Tenerife, Spain

<sup>5</sup>Departamento de Física, CUCEI, Universidad de Guadalajara, Blvd. Marcelino García Barragán 1412, Guadalajara, Jalisco, Mexico

Received date; accepted date

## ABSTRACT

Based on spectrophotometric observations from the Guillermo Haro Observatory (Cananea, Mexico), a study of the spectral properties of the complete sample of 24 blue straggler stars (BSs) in the old Galactic open cluster M67 (NGC2682) is presented. All spectra, calibrated using spectral standards, were re-calibrated by means of photometric magnitudes in the Beijing-Arizona-Taipei-Connecticut system, which includes fluxes in 11 bands covering  $\sim 3500 - 10000 \text{ \AA}$ . The set of parameters was obtained using two complementary approaches that rely on a comparison of the spectra with (a) an empirical sample of stars with well-established spectral types and (b) a theoretical grid of optical spectra computed at both low and high resolution. The overall results indicate that the BSs in M67 span a wide range in  $T_{\text{eff}}$  ( $\sim 5600 - 12600 \text{ K}$ ) and surface gravities that are fully compatible with those expected for main sequence objects ( $\log g = 3.5 - 5.0 \text{ dex}$ ).

**Key words:** stars: blue stragglers — stars: Hertzsprung-Russell (HR) diagram — Galaxy: open clusters and associations: individual: M67

## 1 INTRODUCTION

Blue straggler stars (BSs) were first discovered in the globular cluster M3 by Sandage (1953). These peculiar stars were named ‘blue stragglers’ because of their observational properties in star cluster colour–magnitude diagrams (CMDs). Usually, BSs appear as a bluer and brighter extension of a cluster’s main sequence (MS). As members of the same star cluster and having been born at the same time, the behaviour of BSs is paradoxical because there should be no main sequence stars above the turn-off according to the standard theoretical picture of stellar evolution in such a coeval and initially chemically homogeneous system.

Decades have passed since their discovery, in which they have been the subject of many studies. These peculiar stars have been found to be common constituents of virtually all evolved systems (and also in young systems, but a ‘normally populated main sequence’ would hide any BSs), including dwarf galaxies (Stryker 1993). Based on observational and

theoretical studies, it is generally believed that the BSs in high-density regions of stellar systems could be the remnants of stellar collisions and those in sparse environments might result from the coalescence of interacting binaries or mass transfer through Roche-lobe overflow in primordial binary systems (Ahumada 1999; Bacon et al. 1996; Ferraro et al. 1997; Gilliland & Brown 1992; Leonard 1989; Livio 1993; Ouellette & Pritchett 1998; Piotto et al. 1999; Stryker 1993; Tian et al. 2006). In addition to their still elusive origin, the study of BSs is important because in a stellar population they are among the most massive and luminous stars, whose contribution to the integrated light cannot be predicted by the standard theory of stellar evolution (Bressan et al. 1993). In fact, it has been demonstrated that they greatly affect the spectral energy distribution (SED) of the entire population (Deng et al. 1999; Manteiga et al. 1989), particularly at ultraviolet and blue wavelengths (Xin et al. 2007, 2008).

In spite of the numerous studies published since their discovery, it is still not clear which of the conceivable explanations for the BS phenomenon is the preferred (or dominant) mechanism of formation. Similarly, it has not yet been established whether the spectral properties of BSs are the same as those of regular main sequence stars of the same

\* E-mail: lgq@bao.ac.cn

† E-mail: licai@bao.ac.cn

‡ E-mail: mchavez@inaoep.mx

§ E-mail: ebertone@inaoep.mx

¶ E-mail: ahd@iac.es

**Table 1.** The blue straggler population of M67. ‘n’ is the number of spectra collected for each object.

Name	R.A.(2000)	Dec.(2000)	ExpTime(s)	n
BS005	8:51:11.78	11:45:22.24	2400	4
BS018	8:52:10.75	11:44:06.07	1200	2
BS025	8:51:27.04	11:51:52.22	1200	3
BS029	8:51:48.65	11:49:15.36	2400	4
BS034	8:51:34.31	11:51:10.23	2400	4
BS038	8:51:32.61	11:48:52.02	1200	2
BS040	8:51:26.45	11:43:50.75	1200	2
BS043	8:51:14.37	11:45:00.70	2400	4
BS046	8:51:20.82	11:53:25.65	2400	4
BS047	8:51:03.52	11:45:02.68	1200	2
BS065	8:51:21.77	11:52:38.00	2400	4
BS093	8:51:32.57	11:50:40.42	1200	2
BS111	8:51:19.92	11:47:00.50	1500	2
BS115	8:51:37.72	11:37:03.54	1200	2
BS116	8:50:55.70	11:52:14.50	2400	4
BS126	8:49:21.49	12:04:23.00	1200	2
BS131	8:51:28.40	12:07:38.30	1200	2
BS139	8:51:39.24	11:50:03.66	1500	2
BS143	8:51:21.25	11:45:52.63	1200	2
BS182	8:51:15.47	11:47:31.74	1800	2
BS184	8:50:47.69	11:44:51.33	3300	4
BS185	8:51:28.17	11:49:27.06	3000	4
BS206	8:48:59.84	11:44:51.66	600	1
BS216	8:51:20.59	11:46:16.36	1500	2

mass, as would be expected according to their loci in the CMDs, although this is in contrast to the potential chemical enrichment in the atmospheres presumably provoked by the different detailed formation processes.

Nevertheless, BSs have historically been regarded as core-hydrogen-burning stars (Benz & Hills 1987, 1992). For this reason, it is usually assumed that the spectral properties of BSs are compatible with those of main sequence stars at the same loci in the CMDs. We have adopted this assumption throughout a recent series of papers discussing the integrated SEDs (ISEDs) of star clusters at low spectral resolution (Deng et al. 1999; Xin & Deng 2005; Xin et al. 2007; Xin et al. 2008). However, whether BSs can actually be represented by main sequence objects has not yet been fully investigated, perhaps with the exception of relatively few early papers (Strom et al. 1971). The present paper is therefore aimed at validating this assumption observationally. Determinations are also obtained of the two fundamental parameters, i.e., the effective temperature and the surface gravity, of the full sample of BSs in M67, based on a homogeneous collection of spectra.

With the purpose of properly assessing their nature, we started a long-term project aimed at determining the atmospheric parameters of BSs in stellar systems. We will first determine the effective temperatures and surface gravities of the objects, through photometric and intermediate-resolution spectroscopic observations. In a second step we will investigate the chemical details for (corroboration of) a possible binary nature and to establish the existence (or absence) of the chemical patterns associated with a mass-transfer process.

In this paper we present the initial steps of this project by investigating the full sample of BSs in the well-studied old

**Table 2.** Artificial colours and magnitudes of our sample BSs.

Name	$V$	$B - V$
BS005	10.02	-0.064
BS018	10.68	0.083
BS025	10.95	0.107
BS029	10.93	0.200
BS034	10.95	0.232
BS038	11.10	0.190
BS040	11.29	0.118
BS043	10.94	0.437
BS046	11.22	0.405
BS047	11.34	0.301
BS065	11.32	0.613
BS093	12.27	0.247
BS111	12.16	0.447
BS115	12.33	0.375
BS116	11.99	0.576
BS126	12.22	0.492
BS131	12.60	0.385
BS139	12.28	0.538
BS143	12.30	0.556
BS182	12.71	0.474
BS184	12.72	0.482
BS185	12.82	0.423
BS206	12.92	0.396
BS216	12.92	0.430

open cluster M67 (NGC2682). M67 contains a rich system of 24 BSs (Deng et al. 1999), a sample sufficiently large for statistical purposes. The present paper is organised as follows. In Section 2 we describe the observations. In Section 3 we give the details of the flux-fitting method and provide the final sets of parameters. Fine-tuning of the gravity determination is described in Section 4. In Section 5, a comparison with previous work is presented. Finally, a summary and the conclusions of this study are presented in Section 6.

## 2 OBSERVATIONS AND REDUCTION

The observations were carried out during a three-night run in February 2005 using the 2.12 m telescope of the Guillermo Haro Observatory (OAGH) at Cananea, Mexico. The spectra were collected using the Boller & Chivens spectrograph with a 150  $\ell$ /mm grating blazed at 5000  $\text{\AA}$  and a Tektronix 1024 $\times$ 1024 CCD detector. The instrumental set-up yielded a scale of 3.2  $\text{\AA}$  per pixel with a wavelength coverage roughly from 3600 to 6900  $\text{\AA}$  at a nominal 5.7  $\text{\AA}$  full width at half-maximum (FWHM), with a slit width of 150  $\mu\text{m}$ . A total of 66 object frames were observed, which included at least two frames per object, with the exception of BS206 for which we were able to observe only once.

For the data reduction we followed standard procedures using the IRAF package. Bias and flat-field corrections were secured by collecting a set of ten bias frames as well as dome-projected halogen-lamp images at the beginning and end of each night. Each stellar image was accompanied by a Helium-Argon-lamp image that allowed wavelength calibration and the determination of the nominal resolution along the dispersion axis. The relative flux calibration was done us-

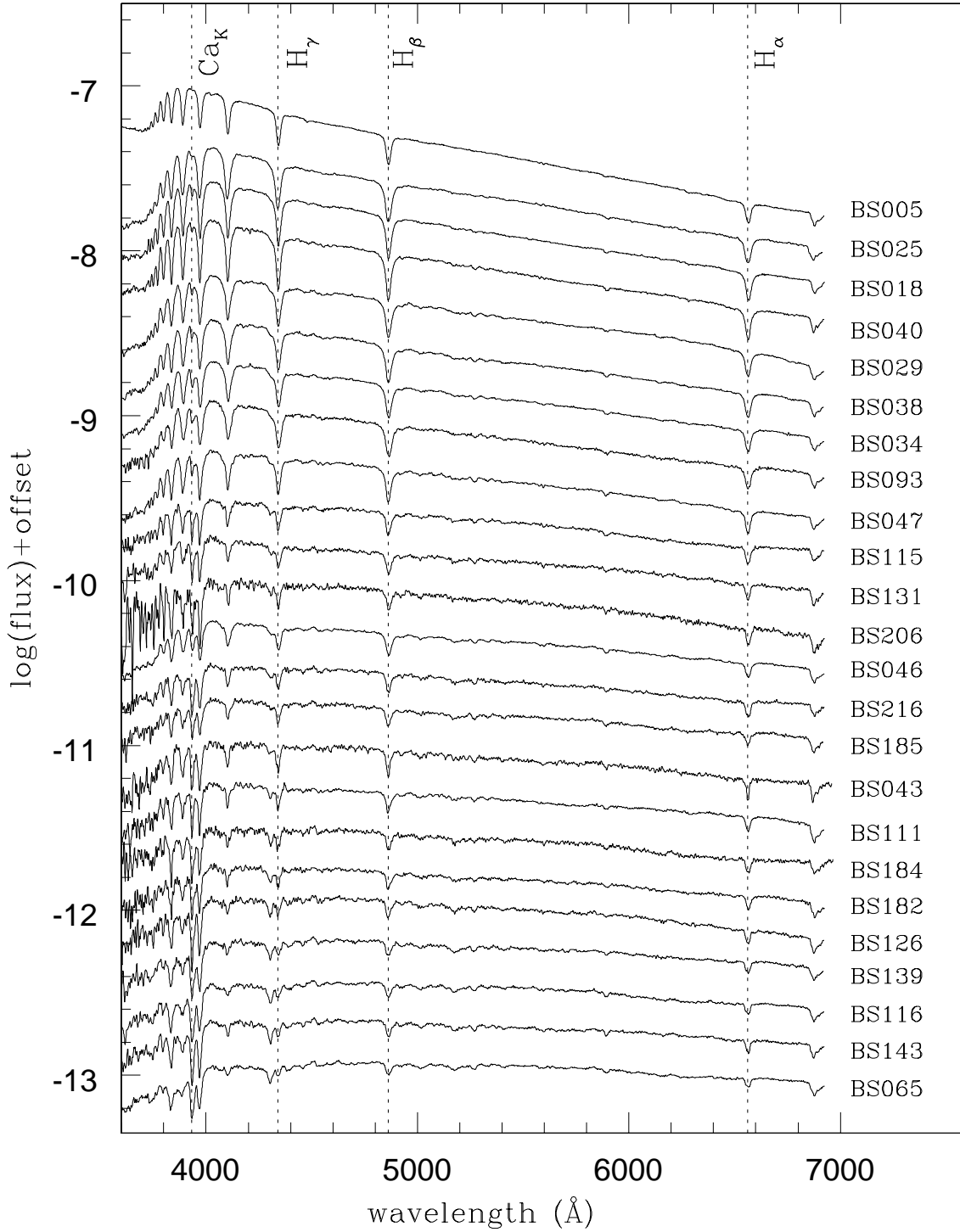


**Figure 1.** Observed spectral energy distributions of the 24 BSs in our sample. The spectra are roughly ordered in a temperature sequence, decreasing from top to bottom. Vertical dotted lines indicate the loci of four major spectral features, H $\alpha$  6562 Å, H $\beta$  4860 Å, H $\gamma$  4340 Å and Ca K 3933 Å.

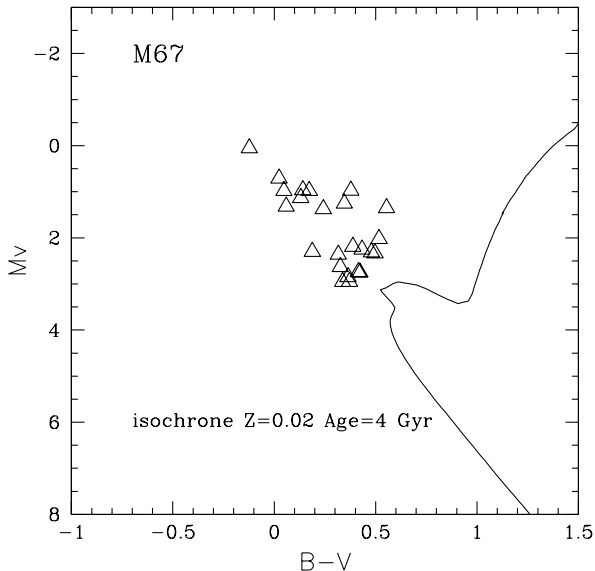


**Figure 2.** Artificial colour-magnitude diagram for the BSs in M67. The full sample of 24 BSs are marked with open triangles. The solid line is the 4 Gyr isochrone of solar metallicity from Bertelli et al. (1994).

ing observations of three spectrophotometric standard stars, BD75325, Feige67, and Feige34.

The 24 BSs in our sample are all members of M67 with nearly 100 per cent membership probabilities, as determined from both proper-motion and radial-velocity observations (Girard et al. 1989; Sanders 1977). The catalogue is included in Table 1 where we give in columns (1) to (5) the BS identification numbers from Fan et al. (1996), the equatorial coordinates, the integrated exposure times (in seconds), and the number of spectra collected for each object. The resulting relative-flux-calibrated spectra are shown in Fig. 1.

Qualitatively, the spectra in Fig. 1 are roughly ordered as a temperature sequence, based on visual inspection of the slope of the SED. It is interesting to note that the sequence of Balmer features, distinguishable down to H11 ( $\lambda = 3771 \text{ \AA}$ ), from bottom to top, exhibits an increase up to BS025, indicating that BS005 should have a temperature compatible with that expected for a late-B star. Similarly, the Ca K line at  $3933 \text{ \AA}$  is nearly absent in the two hottest objects and steadily increases in strength, overcoming the intensity of the blend with He and the Ca H line at  $3968 \text{ \AA}$  at the position of BS184. Another interesting feature easily observable in the spectra is the CH G-band at  $4300 \text{ \AA}$ . This feature is strongest for the two objects at the bottom. Again, from bottom to top, this feature disappears at the position of BS093. Therefore, this star should correspond roughly to spectral type A5 (about  $T_{\text{eff}} = 8000 \text{ K}$ ).

We apply an absolute-flux calibration using intermediate-band photometric data (resembling spectrophotometric observations) collected at an earlier time (Deng et al. 1999). In brief, the 24 BSs were observed photometrically using the Beijing-Arizona-Taipei-Connecticut (BATC) intermediate-band filters. These observations included 11 of the 15 filters in this system, covering a range

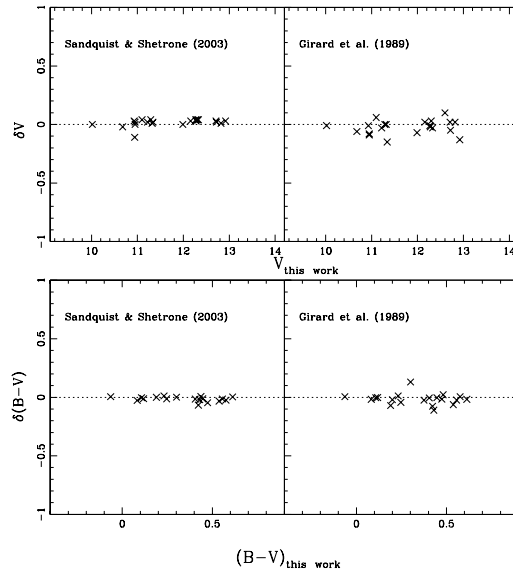


**Figure 3.** A comparison of visual magnitudes (top panels) and  $B - V$  colour indices (bottom panels) of our programme stars between the present paper and those of Sandquist & Shetrone (2003) and Girard et al. (1989).

from  $3500$  to  $10000 \text{ \AA}$ . The shortest wavelength covered by our dataset was obtained using a filter centered on  $3890 \text{ \AA}$ . By convolving the observed BS spectra with the six intermediate-band ( $b, d, f, g, h,$  and  $i$ ; central wavelengths at  $3890 \text{ \AA}$ ,  $4550 \text{ \AA}$ ,  $5270 \text{ \AA}$ ,  $5795 \text{ \AA}$ ,  $6075 \text{ \AA}$ , and  $6660 \text{ \AA}$ , respectively) transmission curves, six new magnitudes for each object were derived. These magnitudes were compared with those obtained with the BATC photometric observations and permitted the derivation of the scaling factors to transform the spectroscopy-based magnitudes to the absolute BATC system. The accurate intermediate-band photometry in the BATC system secures (re-calibrates) the overall shape of the observed spectra for all programme stars.

To assess the quality of the overall SED shapes and to check the precision of the calibration, the spectrophotometrically calibrated spectra were used to construct broad-band photometry, which can then be compared with standard broad-band observations. Two sets of  $V, (B - V)$  observations from Sandquist & Shetrone (2003) – who provided photometric data of BSs in M67 for a study of variability in the light curves – and Girard et al. (1989) – who studied the relative proper motions and the stellar velocity dispersion of M67 – are compared with the artificial magnitudes and colours (see Table 2) of the 24 BSs, derived by convolving the  $B$  and  $V$  filter-response functions with the calibrated spectra. Adopting a distance modulus of  $DM = 9.97 \text{ mag}$  and a colour excess  $E(B - V)$  of  $0.059 \text{ mag}$  for M67 (taken from WEBDA<sup>1</sup>), the observations (both the location with respect to the cluster’s main sequence turn-off and the magnitudes and colours of the programme stars) can very well be reproduced using the artificial CMD photometry, as shown in

<sup>1</sup> <http://www.univie.ac.at/webda/>

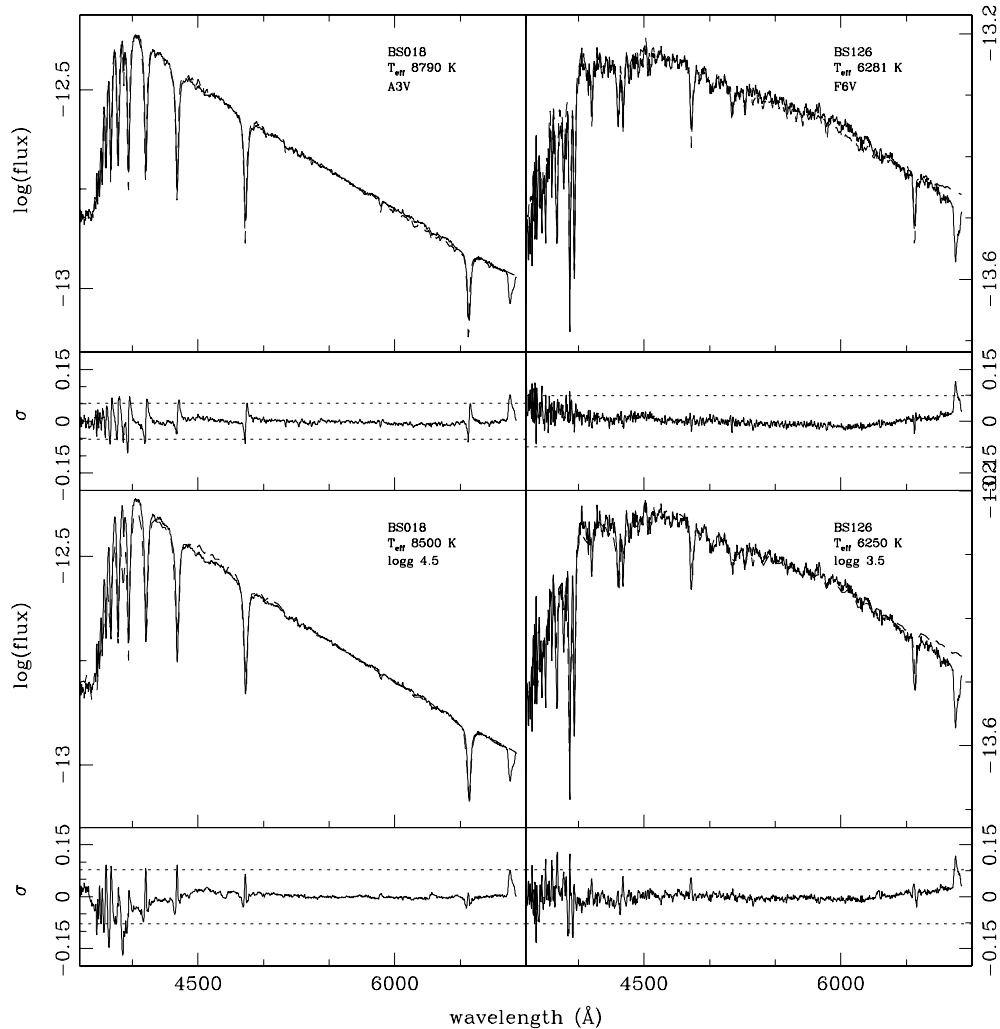


**Figure 4.** Best fits for two representative BSs, BS018 and BS126. The solid and dashed lines show, respectively, the observed spectra and the best-fit Pickles (top panels) and Kurucz low-resolution spectra (bottom panels). The smaller panels below each spectrum correspond to the residuals, as explained in the text, and the dotted lines indicate the  $3\sigma$  boundaries.

Fig. 2. The artificial photometry was also compared with direct broad-band photometry (magnitudes and colours). A perfect match was found, as shown in Fig. 3, in which the residuals in  $V$  magnitude,  $\delta V = V - V_{\text{this work}}$ , and  $(B - V)$  colour index  $\delta(B - V) = (B - V) - (B - V)_{\text{this work}}$  are displayed. No systematic differences were found, whereas the random difference between the data derived from our spectra and from direct photometry is compatible with observational errors of a few per cent of a magnitude. Figure 3 independently shows that our spectral observations and calibration are accurate to a satisfactory degree.

### 3 SPECTRAL FITTING AND ANALYSIS

In order to study the spectral properties of BSs and to determine the effective temperature and surface gravity of our

sample stars, we applied simple flux-fitting methods, using three different libraries of reference stellar spectra, both observed and synthetic. In all cases we assume a solar chemical composition for M67 stars, which is in agreement with observational determinations (Bressan & Tautvaišienė 1996; Hobbs & Thorburn 1991).

(i) Each calibrated spectrum was compared with every entry in the spectral atlas of Pickles (1998). The comparison was carried out after normalising our spectra and those in the reference atlas to the flux at  $\lambda = 5556 \text{ \AA}$ . The algorithm we have implemented finds the spectrum (and its associated parameters) in the atlas that produces the minimum standard deviation,  $\sigma$ , of the residual flux,  $\Delta F = F_{\text{BS}} - F_{\text{Pickles}}$ , computed for each  $\lambda$ .

Because of the marked decrease in sensitivity of the CCD at the shortest wavelengths, the spectral regime considered for the flux fitting excludes the region at  $\lambda < 3850 \text{ \AA}$ . Fig-

ure 4 displays the best fit and residuals for BS018 and BS126 (*top panels*). The solid and dashed lines are, respectively, the BSs’ calibrated spectra and the best-fit flux from the Pickles library. The labels at the top indicate the star ID, its temperature and spectral-type designation.

(ii) A similar procedure was followed by using the spectral grids of Lejeune et al. (1997, 1998) which are, for the segment of the parameter space under consideration, mostly based on Kurucz (1993) low-resolution theoretical fluxes. In this case, both sets of spectra (BSs and model fluxes) were normalised to the flux at  $\lambda = 5390 \text{ \AA}$ . A set of best-fit parameters is found by directly comparing the observed spectra with each of the model fluxes. It is important to note that in this way, as well as in the previous point, the best fit always corresponds to a grid point. In Fig. 4 we show the best fit for the stars BS018 and BS126 (*bottom panels*). The solid and dashed lines are, respectively, the BSs’ calibrated spectra and the best-fit theoretical flux. The label on the right gives the parameters of the best-fit model atmosphere.

(iii) In this case we made use of the BLUERED library (Bertone et al. 2003, 2008). BLUERED is a high-resolution ( $R=500,000$ ) grid of over 800 synthetic stellar spectra, covering SEDs in the optical range ( $\lambda = 3500\text{--}7000 \text{ \AA}$ ). The library is based on the ATLAS9 model atmospheres and has been computed with the SYNTH code developed by Kurucz (1993). The grid spans a large volume in the fundamental parameter space, accounting for virtually any stellar type from O to M stars and from dwarfs to supergiants. An important aspect of this grid, although of marginal relevance for the parameters associated with our programme stars, is that its calculation includes the effect of diatomic molecules, in particular TiO. A best-fit spectrum was found in the two-dimensional space covering ( $T_{\text{eff}}, \log g$ ), after minimising the statistical variance in the relative-flux domain as a measure of the similarity between target spectrum and theoretical SEDs across BLUERED (Bertone et al. 2004). As in the comparisons above, we have assumed a solar chemical composition for M67. It is worth noting that the grid of theoretical spectra has been properly modified to simulate the instrumental set-up. The results are shown in columns (6) and (7) of Table 3, whereas contour plots for BS018 and BS126 are shown in Fig. 5.

The results from the three methods are listed in Table 3, where columns (1) to (8) include, respectively, the object ID, the parameter pairs ( $T_{\text{eff}}, \log g$  or spectral type) and the identification numbers following Sanders (1977), for ease of cross identification.

The agreement among the effective temperature estimates provided by the three methods is on the order of 2–6 per cent and, in general, the best-fit  $T_{\text{eff}}$  values based on the BLUERED library are the highest, apart from the case of the hottest star, BS005, where the best fit is about 1550 K lower. The discrepancy in this case arises from the associated low  $\log g$  value, which is about 2 dex lower than the corresponding result from the Lejeune library, since the flux-fitting method, applied to intermediate-resolution spectra, is affected by a  $T_{\text{eff}}\text{--}\log g$  degeneracy, where a lower surface gravity implies a cooler temperature (Buzzoni et al. 2001).

A larger discrepancy affects the derived surface gravities of our sample stars, for which the highest values are most often provided by the BLUERED library. These latter

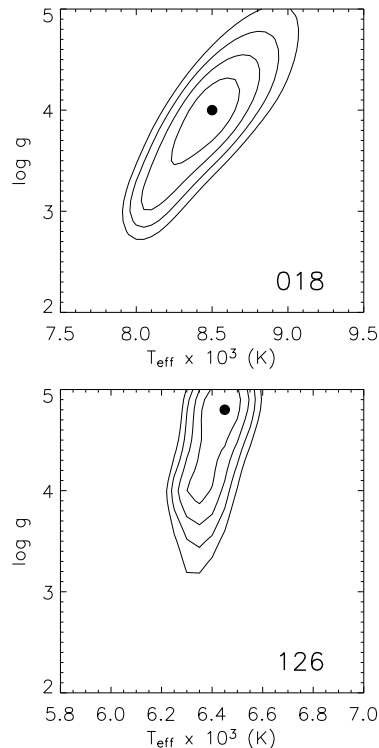


**Figure 5.** Contour plots for BS018 (*top panel*) and BS126 (*bottom panel*). The solid dot corresponds to the best parameter estimate; the contour levels indicate the 1, 2, 3, and  $4\sigma$  uncertainties.

results are, however, affected by an average  $1\sigma$  error of  $\lesssim 1$  dex (see Fig. 5.) The systematically higher parameter values of the BLUERED spectra can be understood as in Bertone et al. (2008), who show that the  $T_{\text{eff}}$  and  $\log g$  values that are obtained from comparing the Sun with the BLUERED spectra (at very high spectral resolution) are a few per cent higher than those commonly accepted because the physical parameters of the absorption lines included in the spectral synthesis generate deeper features – which are counterbalanced by raising both the effective temperature and the surface gravity. In general, the current determinations of gravity for the programme stars are limited by the low resolution.

#### 4 FINE-TUNING OF THE GRAVITY DETERMINATION

Complementary to the analysis presented in the previous section, we obtained observations at OAGH of the BS sample with an alternative set-up that allows, in principle, the separation of potentially fiducial gravity indicators. In particular, we will make use of the indicators defined by Rose (1984, 1994), which consist of line ratios of several pairs of features and the corresponding index-index diagnostic diagrams, and the hydrogen-absorption indices defined by Worthey et al. (1994) as part of the Lick system. These two approaches are necessary in view of the large effective temperature interval covered by the BSs.

New observations were carried out on February 24–27, 2008, using the Boller & Chivens spectrograph and the Ver-

**Table 3.** Best-fit parameters.

<i>Name</i> <sup>a</sup>	BATC-Pickles		BATC-Lejeune		BATC-BLURRED		<i>S</i> <sup>b</sup>
	<i>T</i> <sub>eff</sub> (K)	Sp. Type	<i>T</i> <sub>eff</sub> (K)	log <i>g</i> (dex)	<i>T</i> <sub>eff</sub> (K)	log <i>g</i> (dex)	
BS005	12589	B6IV	12625	5.00	11050	3.1	977
BS018	8790	A3V	8500	4.50	8500	4.0	1434
BS025	8492	A5V	8500	4.25	8950	5.0	1066
BS029*	8054	A7V	7813	4.38	8100	5.0	1267
BS034*	8054	A7III	7688	4.38	7900	5.0	1284
BS038	8054	A7III	7750	4.00	8050	5.0	1263
BS040	8790	A3V	8625	4.75	8450	4.2	968
BS043*	6469	F5V	6500	3.50	6700	4.7	975
BS046*	6776	F2V	6625	3.88	6850	4.7	1082
BS047*	7586	F0III	7250	4.00	7500	4.8	752
BS065	5636	G2V	5750	3.50	6000	4.2	1072
BS093	7586	F0III	7625	4.25	7800	5.0	1280
BS111*	6281	F6V	6500	3.50	6600	4.6	997
BS115*	6776	F2V	7000	4.25	7050	4.7	1195
BS116	6039	F8V	5938	3.75	6150	4.5	792
BS126	6281	F6V	6250	3.50	6450	4.8	277
BS131	6776	F2V	6875	4.75	6950	4.7	1273
BS139	6039	F8V	6000	3.50	6200	4.6	984
BS143	6039	F8V	6000	3.50	6100	4.1	1005
BS182	6281	F6V	6250	4.00	6500	4.7	751
BS184*	6281	F6V	6375	4.25	6500	4.6	1036
BS185	6531	F5V	6438	4.00	6700	4.7	145
BS206	6776	F2V	6750	4.50	6900	4.7	2204
BS216	6531	F5V	6500	4.50	6700	4.7	2226

NOTE: a, Stellar Identification from Fan et al. (1996); b, Sanders number (Sanders 1977); \*, Binary population.

sarray 1300×1300 CCD detector optimised for the blue spectral interval. We used the 600  $\ell$ /mm grating and a slit width of 200  $\mu$ m, which yielded a nominal dispersion of 0.7  $\text{\AA}$ /pixel and a resolution of 2.6  $\text{\AA}$  FWHM. The grating was positioned to obtain spectra in the interval 3800–4700  $\text{\AA}$  where all of the gravity indicators cited above are defined.

The sample consisted of two stellar sets. The first corresponds to the full sample of BSs, whereas the other contains nearly 50 objects that served as gravity templates. The latter set was selected from the catalogues of Cayrel de Strobel et al. (1997, 2001). Data reduction up to the standard flux calibration was performed using the conventional procedures of IRAF and utilising a set of standard stars observed each night. We considered it very important to secure calibrated fluxes to provide reproducible results when analysing data collected with other instruments. In Table 4 we list the control sample, showing in columns (1) to (5) the stellar identification, the spectral type and the associated stellar parameters collected from Cayrel de Strobel et al. (1997, 2001). For the stars with multiple determinations we provide the average values.

As an example of the flux-calibrated spectra we display, in Fig. 6, the lower-resolution spectra of BS065 and a *zoomed-in* region at higher resolution. The vertical dashed lines indicate the position of several of the features used as gravity indicators, as described below.

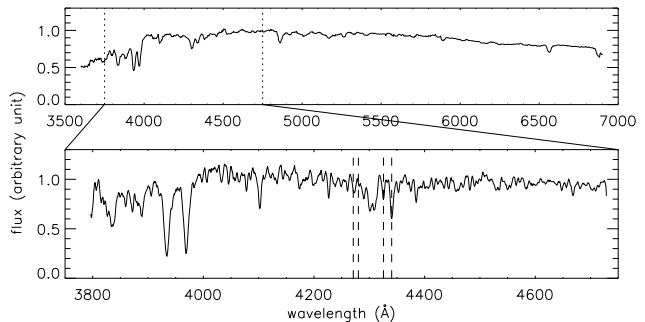


**Figure 6.** Low- (*top panel*) and intermediate-resolution (*bottom panel*) spectra of BS065. The dotted vertical lines indicate the positions of the Rose (1994) features used to define the gravity-sensitive line-depth index used in this paper.

#### 4.1 The wavelength sequence, line ratios and Lick-like indices

We explored all possible combinations of the indices defined by Rose (1994), which are in the form of flux ratios at the central wavelengths of absorption lines or at pseudo-continuum loci, and the Lick/IDS indices (e.g., Worthey et al. 1994; Trager et al. 1998). We visually inspected the spectra of the template stars in search of additional pairs of features that could display a trend with gravity. At the end of the process, the indices that emerged as best gravity diagnostics are (1) the combination 4289/4271 vs. H $\gamma$ /4325

**Table 4.** Stars used as gravity templates.

Name	Sp.Type	$T_{\text{eff}}$ (K)	$\log g$ (dex)	[Fe/H] (dex)
HD025621	F6IV	6251	3.95	0.01
HD027962	A2IV	9000	4.00	0.40
HD028271	F7V	6160	3.85	-0.10
HD028978	A2V	9164	3.70	0.14
HD031295	A0V	8860	4.12	-1.08
HD032537	F0V	6904	4.00	-0.30
HD033256	F2V	6219	3.94	-0.31
HD033608	F5V	6526	4.09	0.23
HD033959	A9IV	7670	3.55	0.00
HD034578	A5II	8300	1.85	0.16
HD035497	B7III	13622	3.80	-0.10
HD035984	F6III	6175	3.68	-0.07
HD038899	B9IV	10903	4.00	0.01
HD043386	F5IV-V	6480	4.27	-0.06
HD061295	F6II	6925	3.00	0.25
HD076292	F3III	6866	3.77	-0.22
HD085235	A3IV	11200	3.55	-0.40
HD087822	F4V	6597	4.10	0.17
HD091752	F3V	6352	3.94	-0.27
HD094028	F4V	5960	4.23	-1.46
HD095418	A1V	9953	4.10	0.47
HD097633	A2V	9395	3.57	0.04
HD099028	F4IV	6739	3.98	0.06
HD099285	F2V	6599	3.84	-0.22
HD100563	F5V	6401	4.31	0.05
HD101606	F4V	6105	4.10	-0.78
HD102574	F7V	6030	3.92	0.16
HD110411	A0V	8970	4.36	-1.00
HD117361	F0IV	6789	3.95	-0.27
HD120136	F6IV	6430	4.19	0.25
HD126660	F7V	6338	4.29	-0.05
HD128167	F2V	6708	4.32	-0.38
HD130945	F7IV	6431	4.06	0.06
HD132375	F8V	6344	4.25	-0.05
HD134083	F5V	6632	4.50	0.10
HD136064	F9IV	6140	4.02	-0.05
HD137052	F5IV	6385	3.91	-0.12
HD139457	F8V	5941	4.06	-0.52
HD142357	F5II-III	6450	3.30	0.20
HD142860	F6IV	6280	4.10	-0.18
HD144206	B9III	11833	3.67	0.01
HD144284	F8IV	6309	4.13	0.20
HD145976	F3V	6720	4.10	0.01
HD150012	F5IV	6380	3.80	0.05
HD155646	F5IV	6179	3.92	-0.14
HD157373	F4V	6420	4.07	-0.48
HD157856	F3V	6309	3.93	-0.18
HD159332	F6V	6184	3.85	-0.23
HD161149	F5II	6600	2.95	0.55

from Rose’s indices, for stars with  $T_{\text{eff}} \leq 7500$  K, and (2) the Lick index  $H\gamma_A$ , for stars hotter than 8000 K.

#### 4.2 Analysis of line-depth ratios

As an important preliminary step, we theoretically verified the sensitivity of all of Rose’s spectral features to surface gravity, in particular those that he identified as discriminators of gravity.

In spite of the similar spectral resolutions, this verifica-

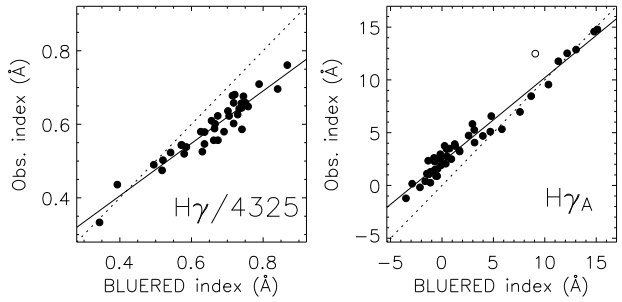


**Figure 7.** Comparisons between the theoretical and empirical indices for the sample of template stars. The empty circle in the right-hand panel corresponds to an object deviating more than  $3\sigma$ . This object was not taken into account for the calibration. The dotted lines show the one-to-one correlations whereas the solid lines denote the best fits.

**Table 5.** Linear transformation parameters.

Index	a	b	rms
4289/4271	0.385	0.605	0.017
$H\gamma/4325$	0.120	0.713	0.026
$H\gamma_A$	2.21	0.80	0.74

tion process is needed because Rose’s spectra were not flux calibrated and, therefore, subject to effects inherent to the particular instrumental set-up he used. In other words, we have corroborated that the selected indices indeed separate the effects of effective temperature from those of gravity.

We calculated the line-depth ratios in a subsample of solar chemical composition synthetic spectra of BLUERED, after properly degrading the grid to match the working resolution of  $2.6 \text{ \AA}$ . As mentioned previously, after exploring the full set of line ratios, we identified the diagnostic diagram including 4289/4271 vs.  $H\gamma/4325$  as the best fiducial combination for differentiating amongst stellar luminosity classes.

Once we have confirmed their sensitivity to gravity, the next step is to transform the theoretical indices to our observational system. For this calibration we compare the theoretical indices with those measured from observed spectra. Note that theoretical values were obtained from BLUERED spectra after linearly interpolating the set of parameters of the template stars (Table 4). As an example of this comparison we show in Fig. 7 the correlations between the theoretical and the empirical indices for  $H\gamma/4325$  and  $H\gamma_A$ . This figure indicates that a linear transformation of the form  $index_{\text{theor}} = a + b \times index_{\text{obs}}$ , suffices to properly match the theoretical and empirical indices.

The comparison resulted in the transformation coefficients listed in Table 5, along with the root mean square error.

In Fig. 8 we display the theoretical diagram (for solar metallicity) for a set of different effective temperatures and gravities, after application of the transformation described above. The dashed and solid lines illustrate, respectively, the iso- $T_{\text{eff}}$  and iso-gravity curves. In the top panel we overplot the loci of the template stars with  $-0.15 \leq [\text{Fe}/\text{H}] \leq +0.15$



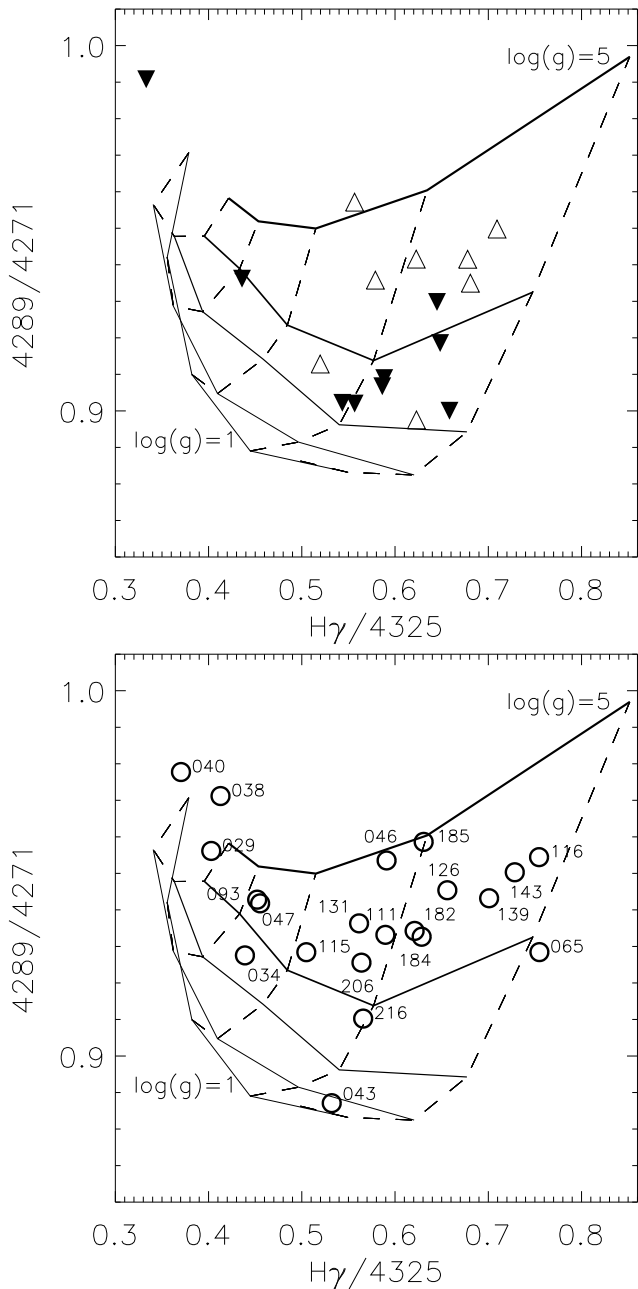


**Figure 8.** Diagnostic diagram for Rose’s indices  $4289/4271$  vs.  $H\gamma/4325$ . Dashed lines indicate the iso- $T_{\text{eff}}$  curves at 6000, 6500, 7000, 7500, 8000, and 8500 K (from right to left), while the solid lines show iso-gravity trends at  $\log g=5, 4, 3, 2$  and 1 dex for the theoretically calculated indices. In the *top panel* the upward and downward triangles indicate, respectively, reference stars with gravities in the intervals  $\log g=4.0-4.5$  dex and  $\log g=3.5-4.0$  dex. In the *bottom panel* the positions of the BSs are marked with open circles, along with their identifications.

dex. In the bottom panel we show the same diagram and the positions of the BSs.

From inspection of the panels in Fig. 8 we note the following characteristics: up to an effective temperature of 7500 K, the indices can clearly be used to separate among stars of the three higher gravity bins, a sensitivity which ap-

pears enhanced for dwarfs and subgiants. Most of the BSs show up in the interval  $\log g=4.0-5.0$ . The only exceptions are BS034, BS043, BS065 and BS216, for which their loci in the diagrams indicate gravities lower than  $\log g = 4.0$  dex. Interestingly, in the work of Mathys (1991) two of these stars, BS034 and BS043, also turned out to be the lowest-gravity objects, with  $\log g=3.79$  and 3.44, respectively, although the latter star might require a more detailed analysis since it is part of a close pair (Girard et al. 1989).

Importantly, we note at this point that we have not (yet) attempted to use these diagrams to derive values for the atmospheric parameters, but instead we only provide an overall assessment of the gravity of the objects. For a more quantitative evaluation, a detailed analysis regarding the adequacy of the model spectra is necessary and still beyond the scope of the present paper. At any rate, it is important to mention that in spite of the potential problems associated with theoretical spectra (see Bertone et al. 2008) the diagrams clearly exhibit (even without prior knowledge of the atmospheric parameters) that most stars with  $T_{\text{eff}} \leq 7500$  K have surface gravities compatible with stars on the main sequence.

### 4.3 The $H\gamma$ Lick-like index

For the BS stars of higher temperatures we have measured absorption indices of the hydrogen Balmer lines, as defined by Trager et al. (1998). We have termed these indices ‘Lick-like’ since they have not been transformed to the Lick system. The overall behaviour of the indices associated with the  $H\gamma$  and  $H\delta$  lines in empirical data has demonstrated that the indices barely depend on metallicity and are very sensitive to gravity for stars with  $T_{\text{eff}} > 8500$  K. We have constructed a theoretical diagnostic diagram of  $H\gamma_A$  vs.  $T_{\text{eff}}$  using BLUERED. In a similar fashion to the line-depth indices, we have calibrated theoretical indices by comparing them to the indices measured in the template stars. The results are included in Table 5. In Fig. 9 we display the theoretical trends for solar chemical composition, with the stars represented as in Fig. 8. In Fig. 9 we include the full sample of template stars regardless of their chemical composition. Note that the index values degenerate at low temperatures, whereas stars are well separated at high temperatures, in particular BS005 (our hottest object). According to this diagram, the three hottest stars have surface gravities in excess of  $\log g=4.0$ , although – because of their temperature – their loci in the diagram do not allow us to precisely establish this parameter. The hot object BS005 appears to have a gravity of about  $\log g=3.6$ , which is compatible with our determination using the BLUERED grid.

There are two objects, BS029 and BS038, that do not lie within the physically expected regions in the two diagrams. For these stars, Mathys (1991) determined effective temperatures consistent with our determination, and gravities of  $\log g=3.91$  and 4.14 for BS029 and BS038, respectively.

Therefore, the spectral properties of BSs can be represented by main sequence stars with the same photometric properties when modeling a simple stellar population based on (photometric) observations of star clusters.

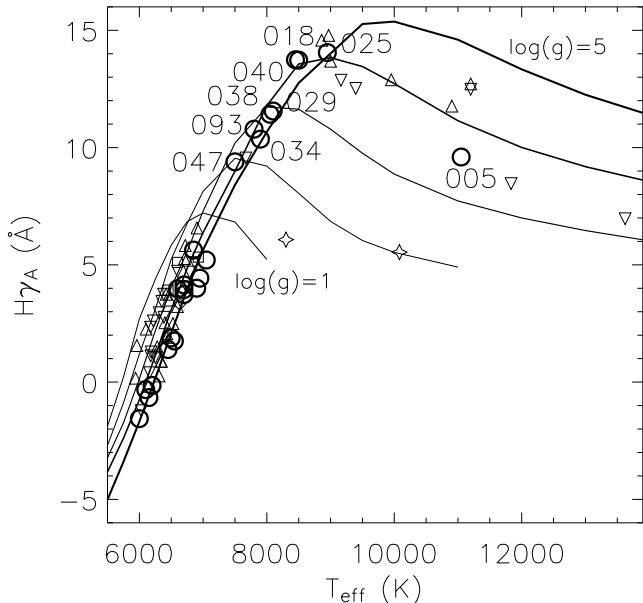


**Figure 9.** Lick-like index  $H\gamma_A$  as a function of effective temperature. The solid lines show the theoretical iso-gravity curves from  $\log g=5$  to 1 dex from solar metallicity spectra. Observed stars are marked with the same symbols as in Fig. 8 with the addition of squares marking objects with  $\log g=2.5\text{--}3.5$  dex and starred symbols denoting stars with  $\log g < 2.5$  dex.

## 5 COMPARISON WITH PREVIOUS WORK

Previous studies of BSs in M67 include, for instance, Bruntt et al. (2007) for BS018, BS025, BS034, BS038, BS040, BS047, and BS093, based on asteroseismic analysis for  $\delta$  Scuti pulsations, and Shetrone & Sandquist (2000) for BS043, BS046, BS139, and BS206, based on abundance analysis. Mathys (1991) analysed 11 BSs in M67 and studies on binarity are also available (see below). However, a homogeneous survey of the full sample of BSs in M67 and complete atmospheric parameter determinations have not yet been carried out. Mathys (1991) presented a spectroscopic study of 11 BSs in M67, and performed a detailed abundance analysis for F 153 and F 185. He concluded that the effective temperatures and surface gravities of the BSs in M67 were quite similar to those of normal main sequence stars of the same spectral type.

There is an obvious difference between his method and ours. Based on the photometric data from Mermilliod (1988), Mathys (1991) derived the atmospheric parameters from the photometric measurements of the BSs in the Strömrgren system, applying the relevant calibration to determine the effective temperatures and surface gravities of B-, A- and F-type stars using *uvby* $\beta$  photometry (Moon & Dworetzky 1985).

The effective temperatures derived from the present work (from BLUERED) for the 11 BSs in common are consistent with Mathys (1991), as shown in Fig. 10(a), and the surface-gravity determinations are less conclusive for most of the BSs compared with Mathys (1991), as shown in Fig. 10(b). The error bars (horizontal axes) in Fig. 10 were obtained based on BLUERED spectral fits, whereas the vertical error bars are from Mathys (1991).

For the 11 BSs in common, the surface gravities of BS005, BS018, BS025, BS038, BS040, BS046, BS047, and BS093 in both papers are in fairly good agreement, considering the error bars. Large deviations in surface gravities are found for the remaining three BSs in common (BS029, BS034, BS043), as shown in Fig. 10(b). Very likely, the undoubted binary nature of these three objects is responsible for the deviations between the two methods.

Indeed, there are eight objects in the list of BSs in M67 which are likely binary candidates, based on previous observations. The BSs identified as binaries are marked by asterisks in Table 3. The BS BS034 (S1284), for instance, is thought to be a binary system in the final stages of mass transfer (Milone & Latham 1992; Zhang et al. 2005). Milone & Latham (1992) considered the dominant light contributor in BS034 to be the original primary (now the secondary) with an orbital period of 4.18284 days and an eccentricity of  $e=0.205$ . Based on high-precision radial velocity measurements, they obtained a spectroscopic orbital solution for the BS binary system. They supposed that the mass transfer began fairly recently and that this BS was formed through stable mass transfer with nearly 100 per cent efficiency. BS046 (S1082) was found to be a complex unusual eclipsing binary system, or even a triple system of which the SED could be explained by the sum of a close binary and another main sequence star (van den Berg et al. 2001; Zhang et al. 2005). BS029 (S1267), BS043 (S975), BS047 (S752), BS111 (S997), and BS115 (S1195) were all identified as spectroscopic binaries with long periods ranging from 800 to 5000 days (Latham & Milone 1996). BS184 (S1036) was detected as a W UMa-type binary with a small amplitude of light variations, and a strong but stable O’Connell effect (Sandquist & Shetrone 2003).

In our work, these binaries were easily fitted using model spectra of single stars. Although we cannot corroborate their binary nature, to within the limited resolution of the observations, we can nevertheless provide constraints on the BSs’ spectral properties.

## 6 SUMMARY AND DISCUSSION

This study represents the first attempt to derive the parameters of the full sample of BSs in the old Galactic open cluster M67 (NGC2682) in a homogeneous way. Low-resolution spectra of the sample of 24 BSs in M67 were collected using the 2.12 m telescope of the Guillermo Haro Observatory (Mexico). The entire data set was re-calibrated using the BATC intermediate-band photometric system, in addition to the usual relative calibration using standard stars, and was subsequently used for a comparison with three different stellar databases aimed at studying their spectral properties in a systematic way. We found that all objects have gravity values in agreement with the expected values for objects in the hydrogen-burning stage.

Considering the original goal of our work, we conclude that, in terms of spectroscopic properties at low resolution, the BSs can indeed be represented by empirical or theoretical data of (or compatible with) main sequence stars, at least in a low density environment as in M67.

As a natural extension to this, it is further concluded that when building up the empirical SEDs of SSPs based

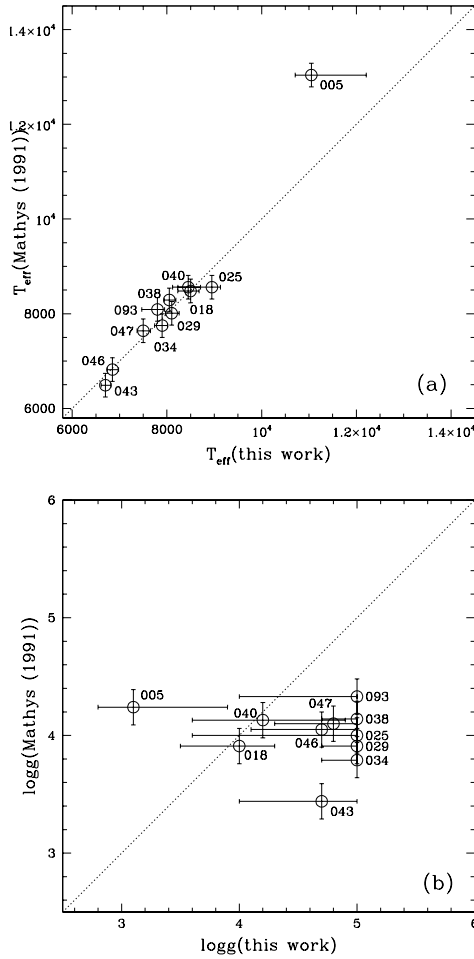


**Figure 10.** Comparison between our results and those of Mathys (1991): (a) effective temperature; (b) surface gravity. The dotted lines are the one-to-one correlations. The open circles are the 11 BSs (labeled by star IDs) in common between the present work and Mathys (1991).

on stellar clusters, the contributions due to BSs can be accounted for using photometry and stellar spectral libraries. This conclusion holds at least at low and intermediate spectral resolution.

Limited by the spectral resolution of the current observational data set, it is not possible to assess binarity and the formation mechanism of the sample of BSs in M67. We anticipate that a detailed chemical abundance analysis at high resolution will show signatures of these dynamical and physical processes. Therefore, the current work serves as a valuable starting point.

**ACKNOWLEDGMENTS**

We thank the anonymous referee for rapid and useful comments. We would like to thank the National Science Foundation of China (NSFC) for support through grants 10573022, and the Ministry of Science and Technology of China through grant 2007CB815406. MC and EB would like to thank CONACYT through grants SEP-2005-49231 and

SEP-2004-47904. We would like to thank Richard de Grijs for language proof reading the paper.

**REFERENCES**

Ahumada J. A., 1999, *RMxAC*, 8, 89  
 Bacon D., Sigurdsson S., Davies M. B., 1996, *MNRAS*, 281, 830  
 Benz W., Hills J. G., 1987, *ApJ*, 323, 614  
 Benz W., Hills J. G., 1992, *ApJ*, 389, 546  
 Bertelli G., Bressan A., Chiosi C., Fagotto F., Nasi E., 1994, *A&AS*, 106, 275  
 Bertone E., Buzzoni A., Rodríguez-Merino L. H., Chávez M., 2003, *Modelling of Stellar Atmospheres*, 210, p. A1  
 Bertone E., Buzzoni A., Chávez M., Rodríguez-Merino L. H., 2004, *AJ*, 128, 829  
 Bertone E., Buzzoni A., Chávez M., Rodríguez-Merino L. H., 2008, *A&A*, 485, 823  
 Bressan A., Tautvaišiene G., 1996, *Baltic Astron.*, 5, 239  
 Bressan A., Fagotto F., Bertelli G., Chiosi C., 1993, *A&AS*, 100, 647  
 Bruntt H., Stello D., Suresh J. C., Arentoft T., Bedding T. R., Bouzid M. Y., Csubry Z., Dall T. H., Dind Z. E., Frandsen S. and 13 coauthors, 2007, *MNRAS*, 378, 1371  
 Buzzoni A., Chavez M., Malagnini M. L., Morossi C., 2001, *PASP*, 113, 1365  
 Cayrel de Strobel G., Soubiran C., Friel E. D., Ralite N., Francois P., 1997, *A&AS*, 124, 299  
 Cayrel de Strobel G., Soubiran C., Ralite N., 2001, *A&A*, 373, 159  
 Deng L., Chen R., Liu X. S., Chen, J. S., 1999, *ApJ*, 524, 824  
 Fan X., Burstein D., Chen J. S., Zhu J., Jiang Z., Wu H., Yan H., Zheng Z., Zhou X., Fang L.-Z. and 16 coauthors, 1996, *AJ*, 112, 628  
 Ferraro F. R., Paltrinieri B., Fusi Pecci F., Cacciari C., Dorman B., Rood R. T., Buonanno R., Corsi C. E., Burgarella D., Laget M., 1997, *A&A*, 324, 915  
 Gilliland R. L., Brown T. M., 1992, *AJ*, 103, 1945  
 Girard T. M., Grundy W. M., Lopez C. E., van Altena W. F., 1989, *AJ*, 98, 227  
 Hobbs L. M., Thorburn J. A., 1991, *AJ*, 102, 1070  
 Latham D. W., Milone A. A. E., 1996, *ASPC*, 90, 385  
 Lejeune Th., Cuisinier F., Buser R., 1997, *A&AS*, 125, 229  
 Lejeune Th., Cuisinier F., Buser R., 1998, *A&AS*, 130, 65  
 Leonard P. J. T., 1989, *AJ*, 98, 217  
 Livio M., 1993, *ASPC*, 53, 3  
 Manteiga M., Martinez R. C., Pickles A. J., 1989, *Ap&SS*, 156, 169  
 Mathys G., 1991, *A&A*, 245, 467  
 Mermilliod J.-C., 1988, *Bull. Inform. CDS*, 35, 77  
 Milone A. A. E., Latham D. W., 1992, *IAUS*, 151, 475  
 Moon T. T., Dworetzky M. M., 1985, *MNRAS*, 217, 305  
 Ouellette J. A., Pritchett C. J., 1998, *AJ*, 115, 2539  
 Pickles A. J., 1998, *PASP*, 110, 863  
 Piotto G., Zoccali M., King I. R., Djorgovski S. G., Sosin C., Dorman B., Rich R. M., Meylan G., 1999, *AJ*, 117, 264  
 Rose J. A., 1984, *AJ*, 89, 1238  
 Rose J. A., 1994, *AJ*, 107, 206  
 Sandage A. R., 1953, *AJ*, 58, 61

- Sanders W. L., 1977, *A&AS*, 27, 89  
Sandquist Eric L., Shetrone Matthew D., 2003, *AJ*, 125, 2173  
Shetrone Matthew D., Sandquist Eric L., 2000, *AJ*, 120, 1913  
Strom S. E., Strom K. M., Bregman J. N., 1971, *PASP*, 83, 768  
Stryker L. L., 1993, *PASP*, 105, 1081  
Tian B., Deng L., Han Z., Zhang X. B., 2006, *A&A*, 455, 247  
Trager S. C., Worthey G., Faber S. M. et al., 1998, *ApJS*, 116, 1  
van den Berg M., Orosz J., Verbunt F., Stassun K., 2001, *A&A*, 375, 375  
Worthey G., Faber S. M., Gonzalez J. J., Burstein D., 1994, *ApJS*, 94, 687  
Xin Y., Deng, L. 2005, *ApJ*, 619, 824  
Xin Y., Deng L., Han Z. 2007, *ApJ*, 660, 319  
Xin Y., Deng L., de Grijs R. et al. 2008, *MNRAS*, 384, 410  
Zhang X. B., Zhang R. X., Li Z. P. 2005, *ChJAA*, 5, 579